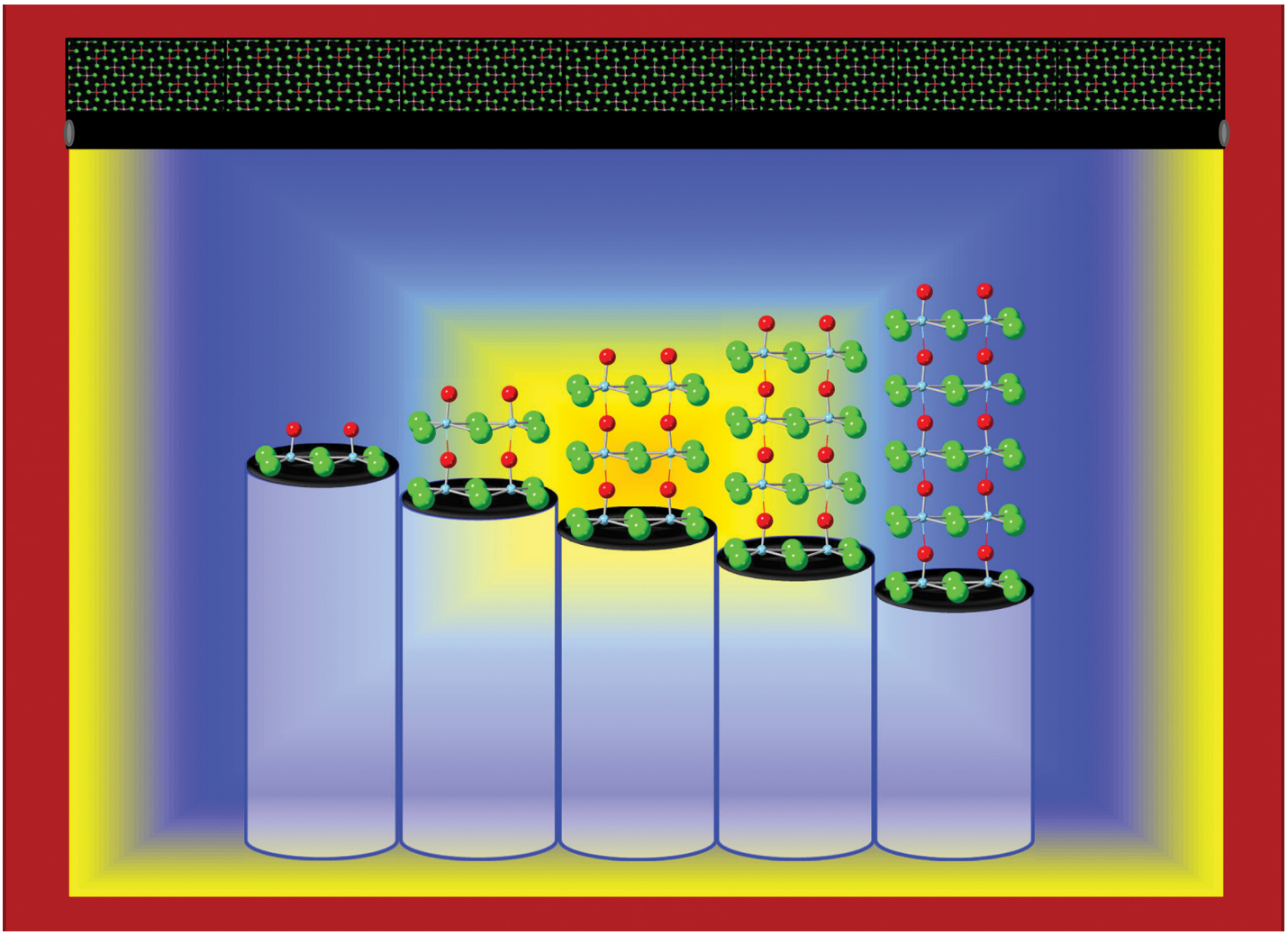

Showcasing research from Professor Kelling Donald's laboratory, Department of Chemistry, University of Richmond, Virginia, United States.

Sigma-hole-supported interactions in complexes of group 5 oxyhalides (MOX_3) with insights for their extended solids

Hoilette Jr., Stewart, and Donald demonstrate that a structural pattern observed in the extended solids of some group 5 oxyhalides – a stacking of dimers that is stabilized by sigma-hole-supported bonding interactions – is already present at the level of the tetramer. The strength of that interaction intensifies, and the average inter-dimer oxygen···metal distance shrinks, as oligomerization, hence the height of the tower, grows. The authors account for or anticipate radical deviations from that 'dimer-tower' motif in other group 5 oxyhalides.

Image reproduced by permission of Kelling J. Donald from *Phys. Chem. Chem. Phys.*, 2026, **28**, 67.

As featured in:

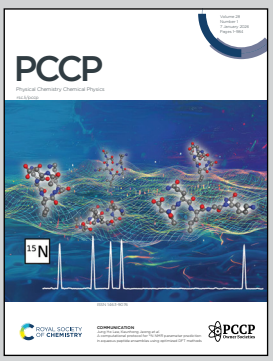

See Kelling J. Donald *et al.*, *Phys. Chem. Chem. Phys.*, 2026, **28**, 67.

PCCP

ROYAL SOCIETY OF CHEMISTRY

PAPER

View Article Online
View Journal | View Issue

Cite this: *Phys. Chem. Chem. Phys.*, 2026, **28**, 67

Sigma-hole-supported interactions in complexes of group 5 oxyhalides (MOX_3) with insights for their extended solids

Donovan Hoilette Jr., Gabriel F. Stewart and Kelling J. Donald *

Received 22nd September 2025,
Accepted 10th November 2025

DOI: 10.1039/d5cp03656a

rsc.li/pccp

The existence and nature of sigma hole type interactions in inorganic extended solids remain largely unexamined, even though the influence of such interactions for heteroorganic compounds is well known. The series of group 5 MOX_3 oxyhalides are intriguing in this regard since several of the known crystal structures are molecular solids with highly polarized M centers. We examine computationally the bonding in the isolated MOX_3 molecules and their smallest clusters $(MOX_3)_n$ where M = V, Nb, and Ta, and X = H, F, Cl, Br, and I. That investigation provides us with substantial evidence, based on patterns and quantitative trends exhibited in the bonding and energetics of the oxyhalide clusters, that several of the extended solids are stabilized by sigma-hole-supported M···O and more rarely M···X bonding interactions between the MOX_3 molecules or dimers. In particular, one-dimensional stacks of doubly bridged, $X_2OMX_2MOX_2$, dimer units in several of the oxyhalide crystal structures are shown to be propagations of sigma-hole-supported bonding interactions with weak charge transfer contributions that are already established at the level of the tetramer. Our results are in harmony with a more recent crystal structure for $NbOCl_3$ over a much older proposal.

Introduction

The relevance of sigma-hole-supported chemical bonding to areas such as crystal engineering is well established.[1–4] The term 'sigma hole interaction' refers to a stabilizing non-covalent interaction achieved when a lone pair on a base, Y, aligns with a localized region of positive electrostatic potential (a positive sigma hole) on a terminal (X) or central (M) atom opposite a polar R–X or R–M bond, respectively. The emergence of a sigma hole on an atomic center is favored if the R group is strongly electron withdrawing; a sigma hole is induced on iodine by $-CF_3$ in F_3C–I, for example, and on carbon (opposite each F–C bond) by F in CF_4.[5,6]

Since the sigma hole on I in F_3C–I or on C in CF_4 arises and is localized immediately opposite the polar C–I or F–C bond(s), sigma hole interactions are optimized when the lone pair on the base is oriented directly toward the sigma hole. So, the R–X···Y or R–M···Y bond angle, such as the C–I···N angle in the F_3C–I···NH_3 complex, is expected to be linear.[7] For bulky and low symmetry donor–acceptor pairs, of course, secondary interactions, such as steric repulsion or competing long range effects, can drive deviations from linearity,[8,9] but such instances are exceptions, as it were, that make the rule.

We use the term sigma-hole-supported bonding for interactions that feature positive sigma holes at the acceptor site in donor–acceptor pairs. In that way, one acknowledges that even if electrostatic contributions (including sigma hole effects) dominate an interaction, charge transfer and other influences on chemical bonding can be substantial. Especially since the sigma holes opposite a bond in an electron acceptor tend to coincide with lobes of empty frontier orbitals, charge transfer and electrostatics are partners, not rivals, in stabilizing weak interactions. In SiF_4, for instance, the four sigma holes on Si – each located opposite a σ_{Si-F} bond – are each coincident with the corresponding σ^*_{Si-F} orbital. So a F_4Si···Y sigma hole interaction is simultaneous with Si ← Y charge transfer such that the bonding in F_4Si ← NR_3 type complexes, for instance,[10–12] is probably best described as a sigma-hole-supported dative bond rather than a sigma hole interaction, especially if NR_3 is a strong base.[6]

Main group systems have received the bulk of the attention in discussions of sigma hole interactions due partly to a significant interest in the properties of organic compounds and complexes and the apparent and potential influences of such interactions in biochemistry, but discussions of sigma hole type interactions involving d-block metals are present in the literature as well.[13–16] Indeed, the obsessive naming of weak

Department of Chemistry, Gottwald Center for the Sciences, University of Richmond, Richmond, Virginia 23173, USA. E-mail: kdonald@richmond.edu; Tel: +1-804-484-1628

sigma hole interactions based on the element or group in the periodic table that is involved has not spared the d-block.[17–19]

One category of transition metal compounds that has become particularly intriguing for the authors is the group 5 oxyhalides. Among those systems, $NbOCl_3$ is one of the best studied. The isolated $NbOCl_3$ molecule may be described as pseudo-tetrahedral about the Nb center such that the Nb═O double bond is along the (vertical) C_3 principal axis and the basal Cl sites are in a horizontal plane. An early experimental crystal structure for $NbOCl_3$[20] revealed an assembly of vertical stacks of $NbOCl_3$ dimers. In that solid, the dimer unit is a di-bridged structure in which one Nb–Cl bond from each monomer is involved in a 3-center 4-electron (3-c, 4-e) Nb–Cl–Nb bridge. The other two Cl atoms on each Nb center in the dimer are roughly coplanar with, but point away from, that bridging region, and the two Nb═O bonds, which are perpendicular to those basal Cl atoms, are parallel or *cis* to each other. So, each Nb center in the dimer is locally five-coordinate (square pyramidal) with the exposed position below both Nb═O bonds vulnerable to attack.

In the stack of dimers found in the extended solid, the Nb═O bonds of one dimer point directly toward those open coordination positions below the Nb═O bonds of a second dimer and so forth. That stacking leads, thus, to a pseudo-octahedral coordination environment around each Nb center in the crystal structure with two apical O and four equatorial Cl atoms. Of note, the distances between the Nb atom and those two apical O sites were determined initially[20] to be equal – suggesting a symmetrization in the bonding (═O···Nb═O → –O–Nb–O–) along the infinite column of dimers. Four decades later, however, a re-examination of the $NbOCl_3$ crystal structure[21] showed that the Nb–O distances are inequivalent, suggesting that the nature of the bonding of Nb to each of the two apical O centers in the pseudo-octahedra is distinct.

In light of the evidence for sigma hole bonding by polarized d-block centers,[13,15,16] and the potential role of sigma holes as ordering influences in main group tetrahedral oxyhalides such as $POCl_3$, and $POBr_3$[22] (and even too in the lower oxidation state systems such as SbOF)[23] we became interested in examining the nature of the chemical bonding in group 5 oxyhalides and related systems. Several of the extended solids of group 5 oxyhalides (MOX_3; for M = V, Nb, and Ta; X = F,[24,25] Cl,[20,21,26,27] Br,[28] and I[28]) are known, and Ault *et al.* have even identified, for instance, ostensibly sigma-hole-supported coordination complexes of VOF_3 and $VOCl_3$ with small bases.[29,30] We investigate the nature of the bonding in the MOX_3 dimers and higher order clusters that lead eventually to the formation of their extended solids. We rationalize the asymmetry identified in ref. 21 and other phenomena in the oxyhalide solids as we probe the role of sigma hole type interactions in fostering if not enforcing structural preferences in extended systems.

Computational methods

All of the molecular species and complexes reported in this work have been optimized using the Gaussian 16 (G16) suite of programs.[31] The systems identified as local minima on their respective potential energy surfaces have been confirmed to be so by harmonic vibrational frequency analyses carried out at the same level of theory and employing the same (superfine) grid, as deployed for the associated structural optimization. All of the computational data presented in this contribution have been obtained using the ωB97XD method,[32] which shows superior performance for the analysis of weak interactions in particular compared to earlier density functional methods.[32] The commonly employed correlation-consistent triple-ζ (cc-pVTZ) basis sets were used for all atoms,[33,34] except for the group 5 metals and iodine. For those elements, in order to manage computational costs while minimizing loss of accuracy, we employed small-core MDF pseudopotentials[35–39] published by the Stuttgart-Cologne group[40] in tandem with the associated triple-ζ basis sets.[41] Electrostatic potential (ESP) maps plotted on the 0.001 a.u. isodensity surfaces have been generated using the Gaussview 6 software[42] within the electrostatic potential range of ±0.05 a.u. on a color spectrum where blue is positive and red is negative. The actual values of the extrema on the potential surfaces were computed using the Multiwfn software package[43,44] and the appropriate output files from the Gaussian 16 calculations. In addition to the GaussView 6 software, the Chemcraft graphical user interface[45] was used to produce representations of molecules and clusters examined in this work. All molecular orbital pictures included in this work were generated using GaussView 6.[42]

Results and discussion

The isolated group 5 MOX_3 molecules (for X = H, F, Cl, Br, or I) have a pseudo-tetrahedral geometry at the central M atom. The M center has a highly positive +5 formal charge, with a M═O double bond and three M–X single bonds. It is expected, therefore, that the M atom will – as is the case for group 14 central atoms in their MF_4 compounds, for example[6] – host four sigma holes: one opposite each bond to the M center. There is a M═O double bond in the systems under consideration here, but the analogy to group 14 molecules is valid since key requirements for four sigma holes, if M is soft enough, are four polarizing σ bonds and no lone pair on the M center.

Given the high electronegativity of O compared to Cl and the heavier halides, the sigma hole opposite the M═O bond is expected to be much stronger in general than those opposite the M–X bonds. For X = F, the situation is harder to predict since F is more electronegative than O.

To move beyond those deductions based solely on chemical intuition, pictures of the computed surface electrostatic potentials, V_s, for the 0.001 au isodensity surface of the MOX_3 molecules were generated and examined (see Fig. 1). For each molecule, the ESP maps are oriented in two ways to show examples of the different types of sigma holes on M: one orientation (top in Fig. 1) exposes the 'O═M•' sigma hole – the sigma hole on M opposite the O═M bond, on the triangular 'X–X–X' face of the MOX_3 pseudo-tetrahedron – with the O atom

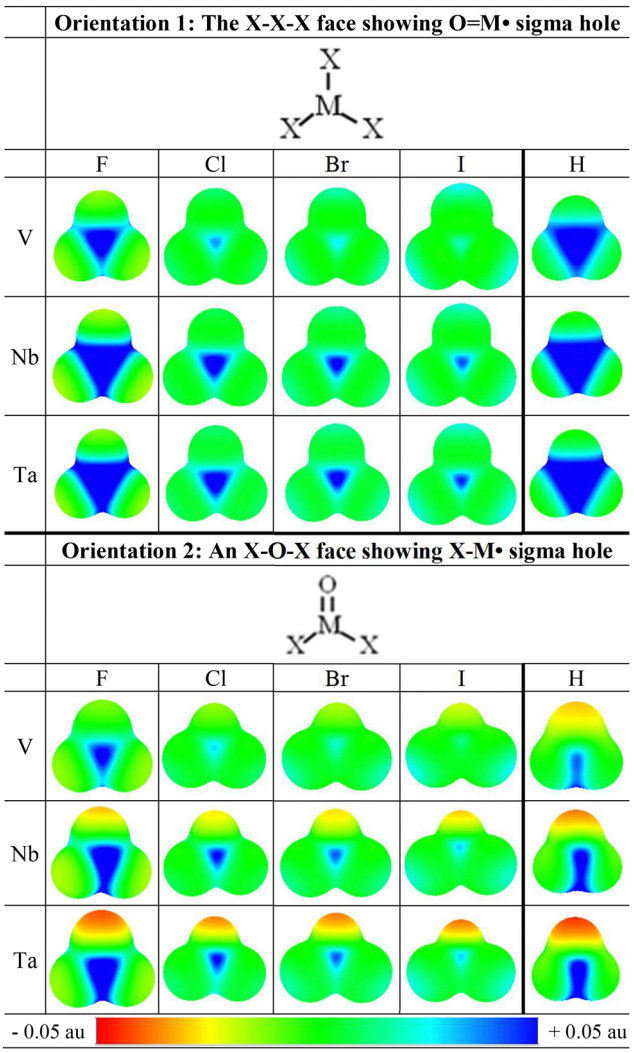

Fig. 1 ESP maps of the group 5 MOX_3 molecules. Two orientations are shown for each molecule, exposing the O═M• sigma hole at the center of the X–X–X face (top), and a X–M• sigma hole on a X–O–X face (bottom) of the molecule.

pointing into the plane of the page; the second orientation (bottom in Fig. 1) shows a 'X–M•' sigma hole – one X–M bond points into the plane of the page such that the sigma hole on M opposite that X–M bond (at the center of a 'X–O–X' face of the pseudo-tetrahedron) is visible. Both views of the molecular surface offer too some faint evidence of the sigma hole on the X atoms (M–X•) as well. Where it exists, that positive halogen atom sigma hole shows up as a faint greenish-blue or light blue region on the halides at the relevant vertices in the ESP maps in Fig. 1, especially for the iodides. The presence of a negative extremum on the ESP surface at the O site is obvious in some of the second (bottom) set of images as a yellow or red region at the top vertex in the ESP maps. F also exhibits a negative extremum, which is betrayed by a faint yellow at the F sites in Fig. 1.

For a more quantitative picture, we computed the values of the maximum in the surface potentials, $V_{s,max}$, at the O═M• and X–M• sigma holes in the MOX_3 molecules, and those values are listed in Table 1 (top, for $V_{s,max}$(O═M•), and bottom for $V_{s,max}$(X–M•) for each M). We determined the ESP minima as well, and we will bring those data into the discussion shortly.

The images shown in Fig. 1 and the $V_{s,max}$ values shown in Table 1 align remarkably well with the deductions outlined earlier based on qualitative chemical intuition. The most positive $V_{s,max}$ values on the isodensity surface of the MOX_3 molecules (the global maxima – in bold in Table 1) arise at the sigma hole on M opposite the O═M bond in every case except for VOI_3. For that oxyiodide (see Table S1(a) and (b)), the sigma hole on I, $V_{s,max}$(V–I•) = 14.9 kcal mol^{-1}, is more positive than any of the other sigma holes induced on that molecular surface: $V_{s,max}$(O═V•) = 11.4 kcal mol^{-1}, and $V_{s,max}$(I–V•) = 7.7 kcal mol^{-1}.

Among all of the oxyhalides, the most positive $V_{s,max}$ values are obtained for the O═M• sigma holes of the oxyfluorides and oxyhydrides (Table 1 and Table S1(a)). Indeed, the $V_{s,max}$(O═M•) values vary with X as follows: F > H ≫ Cl > Br > I (see Table 1), with the single exception being the vanadium case, where (H > F). For each X, the $V_{s,max}$(O═M•) values vary as Ta > Nb ≫ V: for the fluorides, for instance, the $V_{s,max}$(O═V•) is over 30 kcal mol^{-1} weaker than $V_{s,max}$(O═Nb•) and $V_{s,max}$(O═Ta•), which are 81.4 and 82.8 kcal mol^{-1}, respectively – see Table 1. These data are instructive, for they enable us to make certain inferences about the types of bonding interactions that are likely to be most stabilized by sigma hole interactions if the energies and symmetries of frontier orbitals facilitate such interactions. For any given base, for instance, X_3OM ← base complexes of Nb and Ta are expected to establish much stronger sigma hole interactions than their V analogue for any X. And for any M, F and H are predicted to return the most stable complexes.

As we mentioned above, VOI_3 is exceptional, since the sigma hole on the iodine center ($V_{s,max}$(V–I•) = 14.9 kcal mol^{-1}) is larger than both $V_{s,max}$(O═V•) and $V_{s,max}$(I–V•) −11.4 and 7.7 kcal mol^{-1} respectively – on the VOI_3 iso-surface. So, based

Table 1 Values of positive extrema, $V_{s,max}$, at selected sigma holes in the surface electrostatic potentials on M and X on the 0.001 au isodensity surface of group 5 MOX_3 molecules. The value in bold is the most positive of all of the $V_{s,max}$ values for that compound[a]

	σ-Hole	F	Cl	Br	I	H
V	O═M•	**50.4**	**21.9**	**16.3**	11.4[b]	**57.5**
Nb	O═M•	**81.4**	**44.9**	**36.2**	**27.3**	**72.3**
Ta	O═M•	**82.8**	**47.9**	**39.4**	**30.1**	**77.0**
V	X–M•	37.2	17.7	12.8	7.7[b]	25.8
Nb	X–M•	64.5	33.0	26.3	18.9	40.5
Ta	X–M•	64.2	32.8	26.1	18.6	45.1

In each case, the value in bold is the most positive potential in any sigma hole on the isodensity surface of the molecule. [a] Since there are three X–M• sigma holes, we provide the average of the computed $V_{s,max}$(X–M•) values here, and include the standard deviations in the SI: *e.g.*, the average $V_{s,max}$(F–V•) value is 37.16 ± 0.08 kcal mol^{-1}. [b] For VOI_3, the potential maximum at the sigma hole on I, $V_{s,max}$(V–I•) = 14.87 ± 0.01 kcal mol^{-1}, is more positive than $V_{s,max}$(O═V•) = 11.4 kcal mol^{-1}, and $V_{s,max}$(I–V•) = 7.71 ± 0.02 kcal mol^{-1}.

on sigma hole strength alone, halogen bonding may be favored over alternative modes of interaction by VOI_3 as an electron acceptor.

Insights from model heterodimers

To assess the influence of these sigma holes (Fig. 1) on the ability of group 5 oxyhalides and -hydrides to function as acids, and the relationship between the strengths of the sigma holes and the bonding in acid–base complexes of the group 5 compounds, we investigated the structure, bonding and energetics of their trimethylamine (TMA) complexes. To be sure, ammonia is a simpler base for use in model acid–base systems, but less is known about the trimethylamine complexes[30,46] and previous efforts to prepare and analyze $Cl_3OV \leftarrow N(CH_3)_3$ met with frustration[46] so we considered that investigating the latter systems may be useful for comparison with future experimental observations. Key structural and thermodynamic parameters for the optimized C_{3v} $X_3OM\cdots N(CH_3)_3$ complexes are shown in Table 2 and the structural coordinates are included in the SI.

Going down group 5, the atomic radii vary as V < Nb ≈ Ta, which tempts the uninitiated to forecast an increase in M···N bond distances for $X_3OM \leftarrow N(CH_3)_3$ complexes going from M = V to Ta. But the trend in the $V_{s,max}$(O═M•) values shown in Fig. 1 and Table 1 must be considered as well. Notwithstanding the trend in atomic radii, if an intensification of M ← N bonding is sufficiently drastic as M gets larger, an associated contraction in the M···N distance will follow, which may outstrip the difference in atomic radii, with the possible result that the minimum energy M···N distance actually decreases going down group 5 from V to Ta.

The results in Table 2 suggest that precisely such an outcome is achieved in the trimethylamine complexes: the M···N bonds are remarkably short for VOH_3 and VOF_3, but otherwise the interactions strengthen and the M···N distance actually decreases as M gets larger.

A general weakening and elongation of the M···N bond as X gets larger going from F to I in Table 2 correlates with a waning in the strength of the O═M• sigma hole (see Table 1). This is notable, as we consider the prospect for strong charge transfer in the $X_3OM \leftarrow$ TMA complexes, since we find that the gap between the highest occupied molecular orbital (HOMO) of the base (TMA) and the lowest occupied molecular orbital (LUMO) of the MOX_3 acceptor molecule decreases as the halides get larger (see Table S2) – a trend that is expected to promote rather than diminish $X_3OM \leftarrow$ TMA bonding.

For these and other '$O{=}MX_3 \leftarrow$ base' complexes, however, one must acknowledge too the increasingly formidable influence of the X atoms in controlling access to the M center by the base as X gets larger. The base in Table 2 approaches the M center *via* the X–X–X face of the pseudo-tetrahedral $O{=}MX_3$ molecule, and the three X atoms present in effect a physical guard wall to any base aspiring to get beyond that X–X–X face (see Table 2) to the M center of the $O{=}MX_3$ molecule. Going from X = H to F and down group 17 to I, the electron rich X–X–X face becomes increasingly effective in both shielding the M atom – hence masking the O═M• sigma hole – as well as repelling the incoming electron rich base. Consequently, the impact that the substantial polarization of the M center has on dative ($OX_3M \leftarrow$ base) bond formation is weakened as X gets larger, regardless of the suitability of the HOMO–LUMO gap.

Table 2 Geometrical, thermodynamic, and bond order data for the trimethylamine (TMA) complexes of group 5 oxyhalide molecules. Here $\Delta G^{298.15\,K}_{bind.} = G^{298.15\,K}_{Complex} - \left(G^{298.15\,K}_{N(CH_3)_3} + G^{298.15\,K}_{MOX_3}\right)$

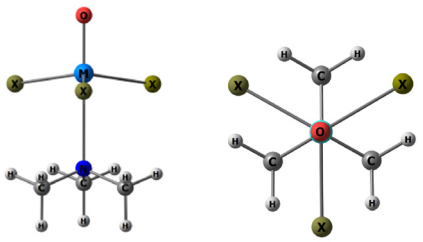

	F	Cl	Br	I	H
	M···N distances/Å				
V	2.527	2.816	2.953	3.105	2.339
Nb	2.589	2.737	2.788	2.841	2.522
Ta	2.580	2.725	2.770	2.816	2.514
	Wiberg bond indices				
V	0.15	0.14	0.13	0.12	0.21
Nb	0.16	0.18	0.18	0.18	0.17
Ta	0.16	0.19	0.19	0.19	0.19
	Binding free energies, $\Delta G^{298.15\,K}_{bind.}$/kcal mol^{-1}				
V	−2.22	3.88	4.33	4.79	−10.25
Nb	−9.81	−3.06	−1.60	0.25	−11.83
Ta	−11.81	−4.56	−3.24	−1.38	−13.57

That insight into the impact of the X–X–X face in limiting the exposure of the base to the highly positive M center helps us to make sense of some of the details of our results. Why, for example, do the hydrides (see Fig. 1 and Table 1) have the strongest or second strongest sigma holes for any M for the MOX_3 molecules? It is definitely not because H is a more electronegative substituent than F, Cl, Br, or even I and thus more effective in enhancing the polarization of M in the MOX_3 species. It is not: on the Pauling scale, χ_P(F) = 3.98, χ_P(Cl) = 3.16, χ_P(Br) = 2.96, χ_P(I) = 2.66, and χ_P(H) is only 2.20! That phenomenon – the exceptionally strong $V_{s,max}$ when X = H – is observed because hydrogen is innocent; the H atom is small and, unlike the halogen X atoms, has no lone pair. So the H–H–H face of the $O{=}MH_3$ molecule allows for the most optimal exposure of the O═M• sigma hole to (hence, access by) an incoming base compared to the other X–X–X faces of the series of MOX_3 molecules.

Indeed, the minimal shielding effect of the H atoms and the slightly smaller size of V relative to Nb and Ta, may account for the curious observation that $V_{s,max}$(O═V•) is actually more positive for VOH_3 than it is for VOF_3. Why is that curious? Although the O═M• sigma hole is attributed formally to polarization of M by O, sigma holes on central atoms (M in this case) are influenced somewhat by all substituents. So – if shielding of the M center by the X–X–X face is weak enough –

the O═M• sigma hole on the O═MX_3 iso-surface is expected to be more positive when X is more electronegative. For M = V, however, the larger size of the F relative to H, and the fact that F has lone pairs, allows the F–F–F face to mask the positive V center enough (Fig. 1) to attenuate the impact of the substantial polarization of V on the net electrostatic potential that arise at the center of the F–F–F face (*i.e.* at M) on the iso-surface. For Nb and Ta, which are a bit larger than V, the F atoms are somewhat less effective at shielding the M center. Consequently, fuller expressions of the O═M• sigma holes (hence more positive $V_{s,max}$(O═M•) values) register on the F–F–F face of the iso-surface for both $NbOF_3$ and $TaOF_3$ such that $V_{s,max}$(O═Nb•) and $V_{s,max}$(O═Ta•) are larger for X = F than they are for X = H (Table 1). For X = Cl, Br, and I, the central M atoms are increasingly more effectively shielded, so the $V_{s,max}$(O═M•) values for X = H are always larger than the $V_{s,max}$(O═M•) values for those larger halides (Table 1) and the X_3OM ← base interactions (see Table 2) weaken accordingly.

Following that analysis, therefore, and given that as the electron rich halogen atoms get larger going from X = F to I the shielding of M by the X–X–X face becomes more substantial, it is hardly surprising that (i) the elongation of the M···N distance in Table 2 is most dramatic (with a change of just over 0.5 Å going from VOF_3 to VOI_3) for the smallest and most easily shielded M atom – vanadium – and that (ii) the OX_3V ← TMA bonding (Table 2) is exergonic for VOH_3 and VOF_3, but increasingly endergonic (Table 2), if still exothermic (Table S3), for X = Cl, Br, and I.

Secondary influences such as any X···H hydrogen bonding between X substituents on Nb and methyl hydrogens in the X_3OM ← TMA complexes may enhance the overall stability of the acid–base pair, but there is no evidence that such interactions play any controlling role in the bonding.

The nature of the orbital interactions contributing to the bonding in the $N(CH_3)_3$ complexes is demonstrated by selected molecular orbitals shown in Fig. 2. The M···N contacts are all in the range 2.33 and 3.11 Å (Table 2), so they are noticeably longer in many cases, especially for the larger halides, than the sums of the covalent radii of M and N[47] – V–N, (1.34 + 0.71) Å = 2.05 Å; Nb–N, (1.47 + 0.71) Å = 2.18 Å; and Ta–N, (1.46 + 0.71) Å = 2.17 Å – but well below the sums of their van der Waals radii – V–N, (2.05 + 1.6) Å = 3.7 Å; Nb–N, (2.15 + 1.6) Å = 3.8 Å; and Ta–N, (2.2 + 1.6) Å = 3.8 Å.[48] So electrostatic interactions are likely to dominate these inter-molecular interactions, and increasingly so as the halogen atom gets larger, M···N elongates, and the already low bond order slowly deteriorates (see Table 2).

Homodimers: a rolling landscape

Our discussion of the X_3OM ← TMA complexes are of interest since some of those pairs have already been studied experimentally[29,30,46] but several others remain to be considered. For this work, however, the homodimers of the metal oxyhalides $(MOX_3)_2$ are of particular interest. As we will see presently, dimer units appear in many of the extended solids of group 5 oxyhalides. 'Vertical' homodimers analogous structurally to the trimethylamine complexes just described (Fig. 2), in which the two monomers establish a X_3M═O···MOX_3 bond mediated by sigma hole and charge transfer interactions, are obtained in this work at the ωB97XD level for only some of the oxyhalide systems. Where it is located, typically for the halides, though never for the fluorides, that homodimer comes with twist. It is somewhat bent as shown in the example on the left (top) in Fig. 3. For X = H and F, the 'vertical' starting structure optimizes with imaginary frequencies that lead us, through subsequent searches, to one of the other structures shown in Fig. 3.

We do not examine the dimer forms in Fig. 3 in detail in this work (see coordinates in the SI), nor do we undertake a more exhaustive or systematic search of the potential energy surface of the homodimers. That is because several of the group 5 MOX_3 extended solid structures feature a distinct form of dimer unit and we take our cue on the bonding motifs that we consider herein from there. Those dimers are held together by a pair of covalent bridging bonds (similar to but more symmetric than the distorted MOH_3 structure in Fig. 3(iii)), and, importantly, sigma hole type interactions appear to be crucial in stabilizing a one-dimensional tower of those dimers, which is a dominant motif in several of the MOX_3 crystal structures.

The extended solids of MOX_3

We have been interested in the donor acceptor properties of group 5 oxyhalides because they hold for us potential insights

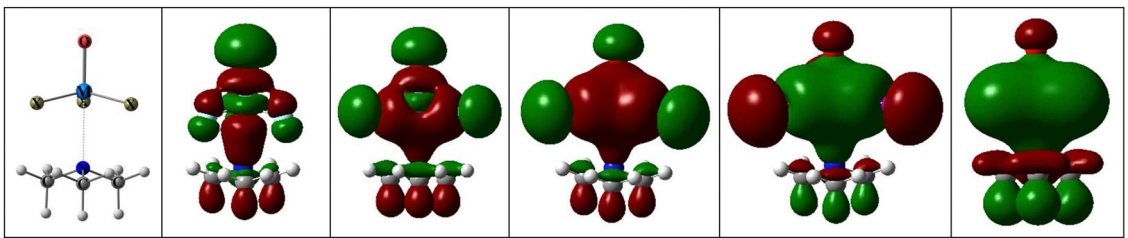

Fig. 2 Representations of X_3ONb ← $N(CH_3)_3$ molecular orbitals that are bonding between the $NbOX_3$ and $N(CH_3)_3$ fragments. The position of each orbital relative to the highest occupied molecular orbital (HOMO) for the complex is indicated. All of the MO pictures share the same orientation. That common orientation is depicted on the left.

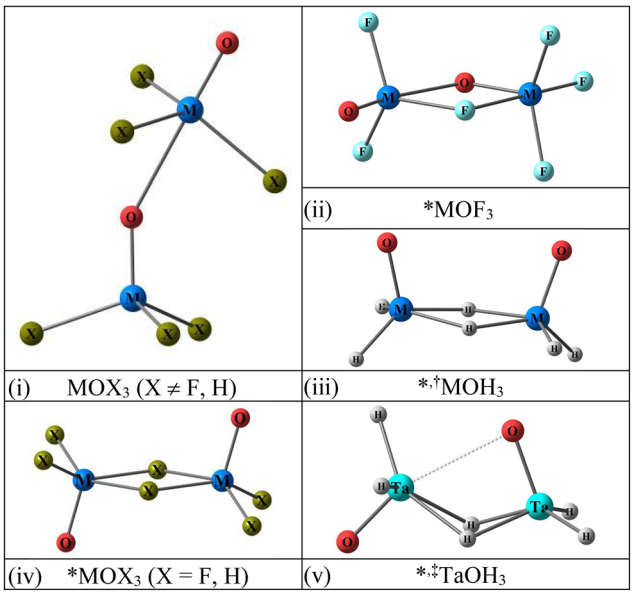

Fig. 3 Diverse minimum energy isomers of MOX_3 dimers obtained from a 'vertical' starting structure. The bent structure (i) is stable for all cases where X ≠ H or F. *The other isomeric forms (ii) to (v) were obtained by following imaginary vibrational frequencies from optimizations for X = F and H. Those forms are not examined further in this work. †For M = Ta, this bridging structure is quite twisted. Far from C_{2v}, the O–M–M–O dihedral is 13.6°. ‡Located only for $TaOH_3$.

into the nature of the bonding present in the $NbOCl_3$ extended solid, for which there have been some ambiguities in the literature.[20,21] We have also been interested more broadly in understanding the potential roles of sigma hole interactions in stabilizing acid–base type interactions in the larger class of group 5 oxyhalides and inorganic extended solids in general.

We have considered the oxyhydride molecules in our discussion so far for completeness, but we have been unable to find crystal structures for any of the group 5 MOH_3 compounds. And many of the oxyhalide crystal structures are missing as well: the oxy-bromides and iodides of V and Ta, and tantalum oxychloride are evidently still unavailable.[49] Representations of published oxyhalide crystal structures are shown in Fig. 4.[49,50] The crystal structures available for $NbOF_3$ and $TaOF_3$ are disordered in the O and F sites and representations of those disordered systems generated using the CrystalMaker modelling program[50] are included in the SI. A published structure with a significant degree of uncertainty in the Nb position in $NbOBr_3$,[28] leading to an average structure that is a symmetrical version of that shown in Fig. 4 is included in the SI as well.

The structures of the MOX_3 solids are interesting (Fig. 4) since the involvement of sigma-hole-supported bonding is apparent in each. Of the known crystal structures, the VOF_3 structure is the only one that exhibits no evidence of M═O···M (or the symmetrical M–O–M) inter-monomer or inter-dimer bonding about the oxygen centers. That vanadium system (top left in Fig. 4) is composed of a network of VOF_3 dimers interlinked by V···F bonds (see the striped bonds in Fig. 4(i)). The dimers are similar to the doubly bridged systems described before ($F_2OVF_2VOF_2$) but with the V═O bonds *trans* relative to a pair of asymmetric 'V–F–V' bridges with bond lengths of 1.920 Å, and 1.972 Å. Those dimers are interlinked by long V···F sigma hole type bonds (2.294 Å) between a terminal F on one dimer and the vacant apical position on the square-pyramidal V site of an adjacent dimer (Fig. 4(i)). That is, the electron rich terminal F atom on one dimer interacts directly with the positive O═V• sigma hole on the second dimer to form a O═V(F_4)···F distorted octahedron.

This observation that VOF_3 is the only crystal structure in Fig. 4 devoid of M···O type inter-monomer or -dimer bonding motivated us to look again at the ESPs on the iso-surfaces of the MOX_3 molecules, focusing in this case on the distribution of ESP minima ($V_{s,min}$). And, remarkably (see Table 3), we find that, in line with the exceptional role of F in the VOF_3 crystal structure, where M···O bonding is absent and M···F interactions dominate, VOF_3 is the only molecule in the whole series in Table 3 in which the negative extremum at F ($V_{s,min}$(M–F►)) is more negative than $V_{s,min}$(M═O►). So, VOF_3 is the single instance for which the global minimum – the most negative spot on the ESP surface – is at the X rather than the O site (see Table S1(a) and (b)).

In the only known $VOCl_3$ crystal structure, dimerization, which was already asymmetrical in the fluoride, is abandoned. The solid is an assembly of antiparallel chains of $VOCl_3$ monomers weakly linked to each other by repeating V═O···V bonds (though published structures disagree a bit on the long intermonomer O···V distance: 3.402 Å[26] and 3.455[27]). In VOF_3, the most substantial ESP extrema (the maximum at O═V• and the minimum at V–F►) drive oligomerization; and that is the case for $VOCl_3$ as well, but in the latter case, the global maximum is again O═V• while the global minimum is V═O► instead of V–Cl► (see Fig. 4(ii), and Table 3).

All of the other crystal structures in Fig. 4 ($NbOCl_3$, $NbOBr_3$, and $NbOI_3$) feature stacks of symmetric dimers with two Nb–X–Nb bridges of equal Nb–X bond lengths. The dimers are arranged in vertical stacks with each dimer linked to the next dimer above it by two Nb═O···Nb contacts. Those long Nb···O bonds – 2.203 Å, 2.210 Å, and 2.233 Å for X = Cl, Br, and I, respectively – are much shorter than the intermonomer V···O contacts in $VOCl_3$ (*vide supra*) a feature that might be anticipated given the escalations in the magnitudes of both $V_{s,max}$(O═M•) and $V_{s,min}$(M═O►) going from M = V to Ta for each X (see Tables 1 and 3). So, the M═O···M interactions between monomer or dimer units in the solids (Fig. 4) are expected to strengthen based on the sigma hole trends alone going down group 5.

Even so, the structural evidence suggests that the double bond character of the M═O bonds is largely preserved in the extended systems (Fig. 4). The short metal–oxygen (Nb═O) distances in the $NbOX_3$ dimer units in the crystal structures, for example, are only 1.758 Å, 1.743 Å, and 1.763 Å for $NbOCl_3$, $NbOBr_3$, and $NbOI_3$, respectively, which are all more than 0.4 Å shorter than the long Nb···O contacts in the crystal structures (*vide supra*; see the striped bonds in Fig. 4), and are within 0.07 Å of the experimental gas phase electron diffraction (r_a)

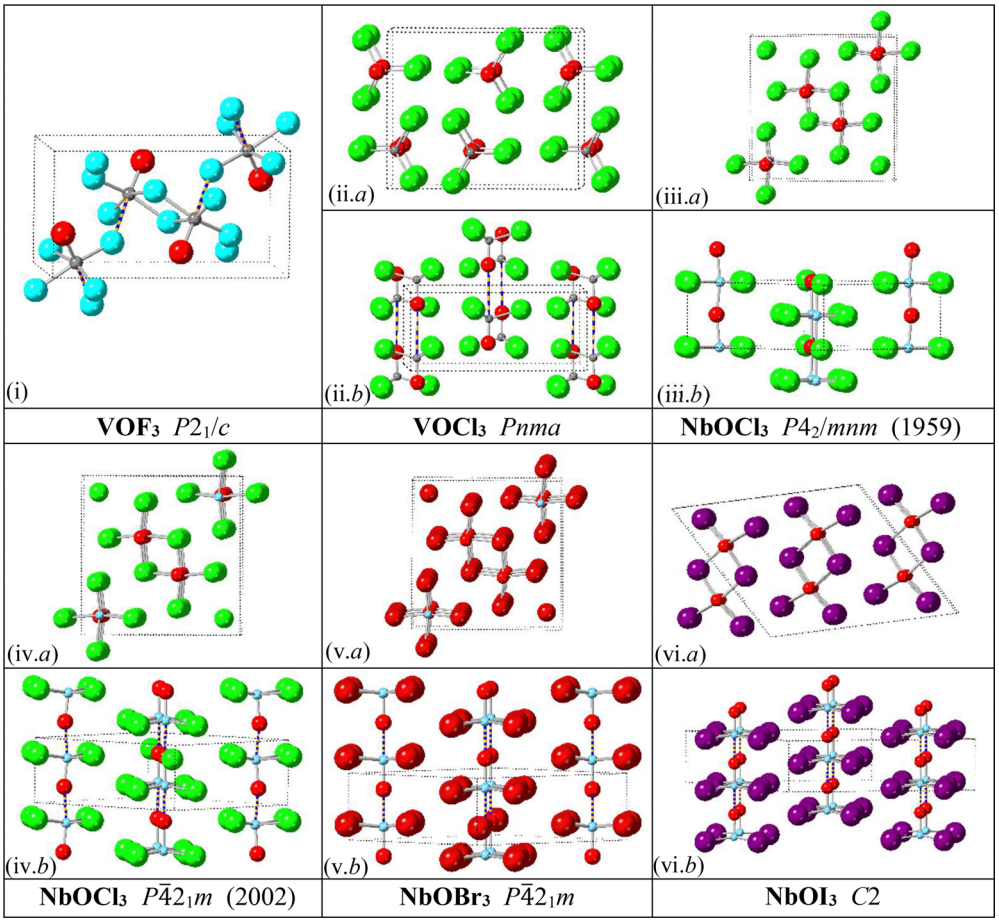

Fig. 4 Images of know crystal structures of group 5 oxyhalides. In most case, two views are presented to brings into focus the layout of one-dimensional stacks as well as the long inter-monomer or -dimer M···O contacts in the solids (striped bonds). Disordered structures published for $NbOF_3$, $TaOF_3$, and $NbOBr_3$ are shown in the SI.

Table 3 Minima of the surface electrostatic potentials in kcal mol^{-1} at O (top) and X (bottom), $V_{s,min}$, on the 0.001 au isodensity surface of group 5 MOX_3 molecules. The value is in bold if it is the most negative (least positive) $V_{s,min}$ value anywhere on the surface of that compound[ab]

		F	Cl	Br	I	H
V	M═O▶	−7.9	**−9.0**	**−10.7**	**−13.1**	**−19.0**
Nb	M═O▶	**−18.8**	**−16.3**	**−17.2**	**−18.3**	**−23.6**
Ta	M═O▶	**−26.1**	**−23.1**	**−23.4**	**−23.9**	**−27.8**
V	M–X▶[b]	**−9.0**	−1.3	−1.8	−1.1	—
Nb	M–X▶[b]	−10.1	−1.2	−1.1	−1.4	−5.6
Ta	M–X▶[b]	−9.1	−1.2	−1.4	+1.7	−5.6

[a] The '▶' symbol is used in this work to indicate an ESP minimum. [b] For the more polarizable X atoms, the local ESP minimum on the atom (M–X▶) arises not opposite the M–X bond but about the electron-rich equator or belt of the X atom. Where different minima appeared at points on that belt, the most negative value was selected. F has no sigma hole (no $V_{s,max}$) in the MOF_3 compounds; in fact, the negative extremum, $V_{s,min}$(M–F▶), is at the pole on F opposite the M–F bond. Each MOX_3 molecule has three essentially identical $V_{s,min}$(M–X▶) values; the average is given in this table and the standard deviation to two decimal places is given in Table S1b.

Nb═O double bond distances in the isolated molecules: 1.693(4) Å, 1.693(7) Å, and 1.717(3) Å.[51] Covalent bonds to central atoms often elongate upon oligomerization or solids formation, especially if the coordination (crowding) around atomic centers increase (such as at M, going from four-coordinate in the MOX_3 molecule to six-coordinate in the solids), so the rather slight increases in the M═O bonds of less than 0.07 Å going from the molecule to the solid signals no grand change in the basic nature of that double bond. What of the nature of the long M···O interaction? As we show in the next section, focusing on the oxyhalides since we have no data for MOH_3 solids, the alternating M═O···M bonding pattern is not exclusively a solid-state phenomenon at all.

MOX_3 bridged dimers

The halogen-bridged dimers identified in many of the extended solids are local minima on the potential surfaces of all of the oxyhalide pairs (see Table 4).[52] In line with a reviewer request, the basic nature of the chemical bonding in such di-bridged structures, and the influence of bridge formation on the M–X distances, is discussed briefly in the SI. The coordinates of the optimized dimers are provided as *.xyz* files in the SI. The free energy changes going from the monomers to the dimers are included in Table 4, and the corresponding enthalpies and

Table 4 $V_{s,max}$(O═M•) and $V_{s,min}$(M═O►) data, all in kcal mol^{-1} units, and binding free energies for the dimers of group 5 oxyhalides relative to isolated monomers

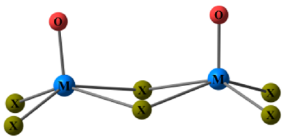

	F	Cl	Br	I
	O═M•			
V	**70.6**	**38.9**	**33.0**	**27.5**[a]
Nb	**98.7**	**67.4**	**58.2**	**48.3**
Ta	**102.2**	**71.4**	**62.0**	**51.9**
	M═O►			
V	−2.0[b]	**−4.7**	**−7.3**	**−10.8**
Nb	**−15.1**	**−13.5**	**−15.0**	**−16.9**
Ta	**−21.5**	**−20.0**	**−21.1**	**−22.5**
	Binding free energies/kcal mol^{-1}			
V	13.3	28.0	27.7	23.0
Nb	−7.6	10.0	12.5	12.9
Ta	−8.6	9.0	11.6	12.8

[a] The sigma hole on I has the most positive $V_{s,max}$ on the iso-surface of the VOI_3 monomer. In the dimer, however, the sigma hole on the terminal iodides ($V_{s,max}$(V–I•) = 13.5 kcal mol^{-1}) is weaker than $V_{s,max}$(O═V•) = 27.5 kcal mol^{-1}. [b] For the VOF_3 dimer, the most negative sites on the iso-surface is that on the pole of the terminal F atoms (opposite the V–F bond) where $V_{s,min}$(M–X►) = −9.5 kcal mol^{-1}. In all other cases, the most negative $V_{s,min}$ value is $V_{s,min}$(V═O►).

zero-point corrected energies are available in Table S4. The strengths of the extrema in the electrostatic potentials at M and O on the dimer iso-surface are included in Table 4 as well.

The bonding is endergonic in these side-on di-bridged dimers, except for Nb and Ta oxyfluorides, but the enthalpies are much more negative (see Table S4). And that structural motif (Table 4) is a minimum on the potential energy surface for all of the oxyhalide molecules, and persist, as we have shown above, in several of the extended solids at ambient conditions. The $V_{s,max}$ and $V_{s,min}$ data summarized in Table 4 (see also Table S5 for the global ESP extrema for each dimer) show that the stacking of the dimer pairs, an acid–base type interaction mediated by two parallel O···M bonds that characterizes the $NbOCl_3$, $NbOBr_3$, and $NbOI_3$ crystal structures in Fig. 4, is strongly favored by the distribution of the electron density in the dimer units.

In those systems, the 'acidic' $V_{s,max}$(O═M•) and 'basic' $V_{s,min}$(M═O►) sites involved in the O···M inter-dimer interactions in the extended solid are the most positive and most negative extrema, respectively, on almost all of the MOX_3 surfaces (Table S5). VOF_3 is the only exception. In that case, $V_{s,max}$(O═V•) is still the most positive extremum, but the minimum on F ($V_{s,min}$(V–F►) = −9.5 kcal mol^{-1}) is much more negative than $V_{s,min}$(V═O►) = −2.0 kcal mol^{-1}. As we pointed out above, a similar observation of a relatively strong negative extremum at F in the free VOF_3 molecule helps us to make sense of the preference for the exceptional and relatively complicated M···X mediated structure in Fig. 4(i) which has no apparent inter-dimer M···O bonding.

MOX_3 tetramers

An assessment of the initial step along the path to the infinite stack of dimers seen in many of the crystal structures is instructive. We find that the basic mode of bonding observed in those solids (Fig. 4) is already present in the tetramer (see Fig. 5). The O sites in the lower bridged dimer in Fig. 5 align with the exposed base of the M atoms of the upper dimer, where the antibonding σ* orbital of the O═M σ bond and O═M• sigma hole of that upper dimer coincide. A model of that type of tetramer structure is shown in Table 5 along with the binding free energies for the pairing process (ΔG_{bind} = G(tetramer) − 2 × G(dimers)), with the corresponding enthalpies and zero-point corrected energies provided in Table S4. The extent of any charge transfer between the two dimers has been quantified as well in the form Wiberg bond indices for the inter-dimer M···O contacts (Table 5).

These results provide the first hint that the patterns found in the extended solids have their roots in some of the smallest clusters of the molecular systems. Indeed, the perception that the oxyfluorides exhibit a distinct behavior compared to the other oxyhalides is also evident in the tetramer as a non-linear stacking of the dimer pairs for M = Nb and Ta (Fig. 5). The tetramer is also tilted for $VOCl_3$, but for VOF_3 the departure is even more elaborate. Neither the linear nor the tilted tetramer is a minimum. Instead, a lower symmetry tetramer (see the SI) was found in which one dimer is displaced horizontally relative to the other. So, we begin to see already that, as oligomerization progresses toward the extended solid, VOF_3 will go its own way.

Insights from higher order oligomers for $NbOCl_3$

The published $NbOCl_3$ crystal structures shown in Fig. 4 (cases (iii) and (iv)) disagree on the (a)symmetry of the Nb–O–Nb inter-dimer contacts. That ambiguity was likely due to high uncertainties in the atomic positions in the early symmetric proposal,[20] which were resolved several decades later.[21] That the bonding in the isolated tetramer of $NbOCl_3$ (Fig. 5) is clearly remembered in the extended solid (Fig. 4), is strong evidence that the observed distortion or asymmetry in the columns of dimers in the crystal structures is not due to any phenomenon specific to the solid state. Rather, it is a culmination of a pattern initiated at the tetramer based ostensibly on sigma-hole-supported bonding interactions with weak though not insignificant charge transfer components (see bond indices in

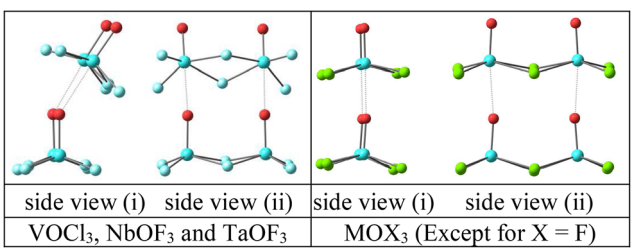

Fig. 5 MOX_3 tetramers built up from bridged dimers; showing $NbOF_3$ (left) and $NbOCl_3$ (right). The tetramer is tilted for $VOCl_3$, $NbOF_3$, and $TaOF_3$. This basic motif is not a minimum for VOF_3.

Table 5 Selected bonding, geometrical, and free energy data for the group 5 oxyhalide tetramers (stacked di-bridge dimer pairs). The distances between the metal atom (^{u}M) in the 'upper' dimer and the oxygen site (^{l}O) in the 'lower' dimer are listed. The binding free energies are computed relative to isolated dimer pairs ($\Delta G^{298.15\,K}_{bind.} = G^{298.15\,K}_{tetramer} - 2G^{298.15\,K}_{dimer}$)

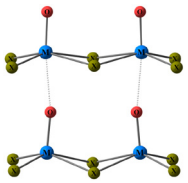

	F[a]	Cl	Br	I
	^{u}M···^{l}O bond distance/Å			
V	[b]	2.983[ac]	2.825	2.810
Nb	2.566	2.573	2.559	2.563
Ta	2.493	2.481	2.463	2.463
	^{u}M···^{l}O Wiberg bond indices			
V	[b]	0.06[a]	0.10	0.13
Nb	0.13	0.19	0.20	0.21
Ta	0.16	0.22	0.24	0.24
	Binding free energies/kcal mol^{-1}			
V	[b]	+5.4[a]	+3.6	0.0
Nb	−5.2	−4.4	−5.3	−8.5
Ta	−16.1	−13.7	−16.8	−22.6

[a] The Nb and Ta fluorides and $VOCl_3$ have C_s symmetry. In those cases, one dimer is tilted relative to the other – a tetrameric version of the bent vertical dimers (Fig. 3(i)). The two inter-dimer M···O bonds are retained as well as the mirror plane passing through the four bridging X atoms. [b] This tetrameric structure is not a minimum for VOF_3. [c] There was a slight difference between the two V···O bonds with an average of 2.9826 ± 0.0015 Å.

Table 5). To assess that inference, we obtained and examined optimized geometries of the hexamer, octamer, and decamer of $NbOCl_3$ in the stacked dimer motif (Table 6).

The coordinates for all of those oligomers are included in the SI. Costly density functional calculations that we performed on the $NbOCl_3$ oligomers up to the decamer prove illuminating. They afford us some useful insights into the evolution of structural and energetic properties of the clusters en route from the doubly bridged dimer units to the extended solids. A clear trend towards shorter average interatomic separations, a slow but steady increase in bond orders, and an escalation of the binding free energies relative to the free dimers are illustrated in Fig. 6.

There is a limited number of data points (from the tetramer to the decamer) for the bond order and bond distance values, but a logarithmic relationship provides the best fit in those cases. A quadratic function affords a surprisingly impressive fit to the free energy as a function of n, and a linear relationship with a high coefficient of determination is found for a theoretical average increase in the stabilization per dimer as the oligomer grows. We find that for each successive dimer added – up to the decamer at least – more stability is conferred on the entire system (Fig. 6(i)). And that stabilization comes with a marginal increase in charge transfer, estimated here by computed bond orders, and a net contraction in the mediating Nb···O contacts.

The structural motif in $NbOCl_3$ and in the isomorphic $NbOBr_3$, and $NbOI_3$ systems shown in Fig. 4 may be described, therefore, as the assembly of oligomeric towers of dimers, where each tower is an expansion on a pattern of bonding already inaugurated at the tetramer and propagated by exergo-

Table 6 Bonding and thermodynamic data for higher oligomers of the $NbOCl_3$ molecule[a]

Hexamer	Octamer	Decamer
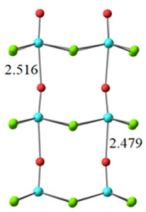	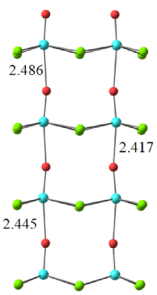	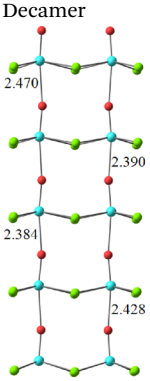
Shortest intermonomer contacts/Å		
2.479	2.417	2.384
Wiberg bond indices		
0.23	0.26	0.27
$\Delta G^{298.15\,K}_{olig.} = G^{298.15\,K}_{n\text{-}mer} - \left(\frac{n}{2}\right) \cdot G^{298.15\,K}_{dimer}$/kcal mol^{-1}		
−11.6	−21.2	−33.4

[a] The corresponding values for the tetramer are included in Table 5 but are echoed here for direct comparison: Nb···O distance: 2.573 Å; bond order: 0.19; $\Delta G^{298.15\,K}_{olig.} = -4.4$ kcal mol^{-1}.

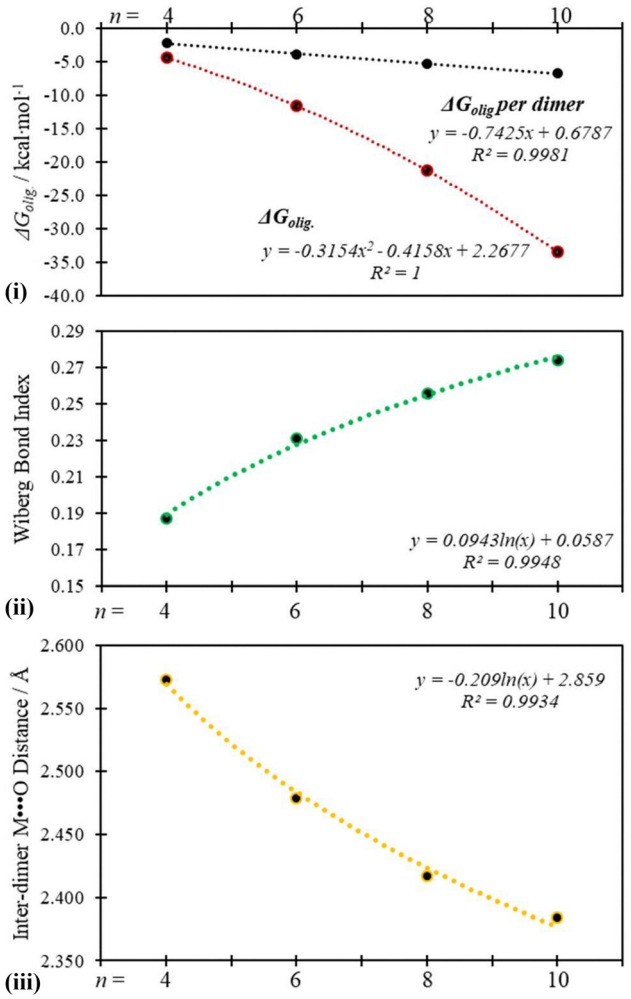

Fig. 6 Illustrations of the dependence of certain bonding and thermodynamic properties of $NbOCl_3$ clusters on oligomer size. (i) Total oligomerization free energies at 298.15 K, $\Delta G^{298.15\,K}$, for oligomerization relative to the dimer units ($\Delta G = G_{n\text{-mer}} - (n/2) \times G_{dimer}$), and per dimer ($\Delta G/(n/2)$). (ii) Wiberg bond orders, and (iii) Inter-dimer M···O distances.

nic sigma-hole-supported interactions. Those interactions become more stabilizing and ever so slightly more dative as stacking progresses. The double bond character of the M═O bonds in the dimer units, however, persists. So covalent inter-dimer M–O–M bridges are never achieved,[53] but the sub-covalent M···O distance definitely contracts as oligomerization progresses (Fig. 6(iii)) through to the extended solid, culminating, for $NbOCl_3$, at 2.203 Å.

Summary and conclusion

Molecular clusters and solids of inorganic compounds remain a rich area for exploration in efforts to enhance our understanding of the nature, role, and potential applications of weak interactions. The group 5 MOX_3 oxyhalides utilize such interactions to stabilize molecular aggregation and extended solid formation. We have shown here that the bonding motif exhibited by many of the group 5 oxyhalide solids are already evident at the level of the tetramer, which is a stack of doubly bridged dimers held together by electrostatic (sigma hole) and weak charge transfer interactions. The charge transfer contribution, based on bond order and structural data, increases gradually as oligomerization progresses, one additional dimer after another, though the alternating non-covalent and double bond $[\cdots M{=}O]_n$ motif never symmetrize to a chain $[-M-O-]_n$ of identical M–O bonds. Sigma hole interactions play a significant role in sustaining the stacked dimer structures. We surmise, however, that weak orbital interactions may help to account for subtle structural features such as the tilting or bending in certain dimer and tetramer isomers. Vanadium oxyfluoride is in a class of its own as an extended solid compared to the other known group 5 oxyhalides. And its exceptional features – in particular an exclusive role for V···F inter-dimer interactions – are traced back to the distribution of electron density in the VOF_3 monomer, for which the global minimum in the electrostatic potential resides on the F center (rather than on the O site, as in the other group 5 MOX_3 molecules).

Author contributions

D. H. Jr.: methodology, computational studies, data curation, analysis, writing preliminary drafts of sections of manuscript, and reviewing: G. F. S.: methodology, computational studies, data curation, analysis, and reviewing K. J. D.: conceptualization, supervision, methodology, computational studies, data curation, analysis, writing, reviewing, editing.

Conflicts of interest

There are no conflicts to declare.

Data availability

The data supporting this article have been included as part of the SI. Supplementary information: includes several visualizable *.xyz* files for systems considered in this work, additional thermodynamic and other data mentioned in the text, images of crystal structures, and the full long reference of the Gaussian 16 software used in completing work leading to results presented in this manuscript. See DOI: **https://doi.org/10.1039/d5cp03656a**.

Acknowledgements

Our work was supported by the National Science Foundation [NSF-RUI Award (CHE-2055119) and NSF-MRI grants (CHE-0958696 (University of Richmond) and CHE-1662030 (the MERCURY consortium))] and by the Henry Dreyfus Teacher-Scholar Awards Program [TH-16-015]. K. J. D. acknowledges as well the support of the University of Richmond (UR) and the Clarence E. Denoon Jr. Endowment in the Natural Sciences at UR.

References

1 C. B. Aakeroy and K. R. Seddon, The Hydrogen Bond and Crystal Engineering, *Chem. Soc. Rev.*, 1993, **22**, 397.
2 P. Metrangolo, G. Resnati, T. Pilati and S. Biella, Halogen Bonding in Crystal Engineering, *Struct. Bonding*, 2008, **126**, 105–136.
3 A. Mukherjee, S. Tothadi and G. R. Desiraju, Halogen Bonds in Crystal Engineering: Like Hydrogen Bonds yet Different, *Acc. Chem. Res.*, 2014, **47**, 2514–2524.
4 A. Frontera and A. Bauzá, On the Importance of σ-Hole Interactions in Crystal Structures, *Crystals*, 2021, **11**, 1205.
5 K. J. Donald, B. K. Wittmaack and C. Crigger, Tuning σ-Holes: Charge Redistribution in the Heavy (Group 14) Analogues of Simple and Mixed Halomethanes Can Impose Strong Propensities for Halogen Bonding, *J. Phys. Chem. A*, 2010, **114**, 7213–7222.
6 K. J. Donald and M. Tawfik, The Weak Helps the Strong: Sigma-Holes and the Stability of MF_4•Base Complexes, *J. Phys. Chem. A*, 2013, **117**, 14176–14183.
7 S. L. Stephens, N. R. Walker and A. C. Legon, Internal Rotation and Halogen Bonds in $CF_3I\cdots NH_3$ and $CF_3I\cdots N(CH_3)_3$ Probed by Broadband Rotational Spectroscopy, *Phys. Chem. Chem. Phys.*, 2011, **13**, 20736–20744.
8 A. J. Parker, J. Stewart, K. J. Donald and C. A. Parish, Halogen Bonding in DNA Base Pairs, *J. Am. Chem. Soc.*, 2012, **134**, 5165–5172.
9 O. S. Bushuyev, D. Tan, C. J. Barrett and T. Friscic, Fluorinated Azobenzenes with Highly Strained Geometries for Halogen Bond-Driven Self-Assembly in the Solid State, *CrystEngComm*, 2015, **17**, 73–80.
10 A. A. Ennan and B. M. Kats, Silicon Tetrafluoride Adducts, *Russ. Chem. Rev.*, 1974, **43**, 539–550.
11 B. S. Ault, Matrix-Isolation Studies of Lewis Acid/Base Interactions: Infrared Spectra of the 1:1 Adduct SiF_4•NH_3, *Inorg. Chem.*, 1981, **20**, 2817–2822.
12 T. J. Lorenz and B. S. Ault, Matrix-Isolation Studies of Lewis Acid/Base Interactions. 2. 1/1 Adduct of SiF_4 with Methyl-Substituted Amines, *Inorg. Chem.*, 1982, **21**, 1758–1761.
13 C. Chieh, Synthesis and Structure of Dichlorobis(Thiosemicarbazide)Mercury(II), *Can. J. Chem.*, 1977, **55**, 1583–1587.
14 Ref. 13 is mentioned in ref. 15 as an earlier example of what is putatively a sigma hole interaction to a Hg center. In that system, the Hg center is pseudo-tetracoordinate with two short Hg–S bonds (<2.42 Å) and two short Hg–Cl bonds (<2.83 Å) but features as well two somewhat longer Cl···Hg contacts (3.250(3) Å), stabilized evidently by sigma hole type interactions.
15 J. Joy and E. D. Jemmis, Designing M-Bond (X-M···Y, M = Transition Metal): σ-Hole and Radial Density Distribution, *J. Chem. Sci.*, 2019, **131**, 117.
16 S. Scheiner, Participation of Transition Metal Atoms in Noncovalent Bonds, *Phys. Chem. Chem. Phys.*, 2024, **26**, 27382–27394.
17 J. H. Stenlid, A. J. Johansson and T. Brinck, σ-Holes and σ-Lumps Direct the Lewis Basic and Acidic Interactions of Noble Metal Nanoparticles: Introducing Regium Bonds, *Phys. Chem. Chem. Phys.*, 2018, **20**, 2676–2692.
18 A. Bauzá, I. Alkorta, J. Elguero, T. J. Mooibroek and A. Frontera, Spodium Bonds: Noncovalent Interactions Involving Group 12 Elements, *Angew. Chem., Int. Ed.*, 2020, **59**, 17482–17487.
19 I. Alkorta, J. Elguero and A. Frontera, Not Only Hydrogen Bonds: Other Noncovalent Interactions, *Crystals*, 2020, **10**, 180.
20 D. E. Sands, A. Zalkin and R. E. Elson, The Crystal Structure of $NbOCl_3$, *Acta Crystallogr.*, 1959, **12**, 21–23.
21 M. Ströbele and H.-J. Meyer, Neubestimmung Der Kristallstruktur von $NbOCl_3$, *Z. Anorg. Allg. Chem.*, 2002, **628**, 488–491.
22 P. R. Varadwaj, A. Varadwaj, H. M. Marques and K. Yamashita, The Phosphorus Bond, or the Phosphorus-Centered Pnictogen Bond: The Covalently Bound Phosphorus Atom in Molecular Entities and Crystals as a Pnictogen Bond Donor, *Molecules*, 2022, **27**, 1487.
23 A. Åström and S. Andersson, The Crystal Structure of L-SbOF, *J. Solid State Chem.*, 1973, **6**, 191–194.
24 J. Supeł, U. Abram, A. Hagenbach and K. Seppelt, Technetium Fluoride Trioxide, TcO_3F, Preparation and Properties, *Inorg. Chem.*, 2007, **46**(14), 5591–5595.
25 J. Köhler, A. Simon, L. van Wüllen, S. Cordier, T. Roisnel, M. Poulain and M. Somer, Structures and Properties of $NbOF_3$ and $TaOF_3$—with a Remark to the O/F Ordering in the SnF_4 Type Structure, *Z. Anorg. Allg. Chem.*, 2002, **628**, 2683–2690.
26 J. Galy, R. Enjalbert, G. Jugie and J. Strähle, $VOCl_3$: Crystallization, Crystal Structure, and Structural Relationships: A Joint X-Ray and 35Cl-NQR Investigation, *J. Solid State Chem.*, 1983, **47**, 143–150.
27 S. I. Troyanov, Crystal Structures of $SbCl_5$, VCl_4, and $VOCl_3$, *Russ. J. Inorg. Chem.*, 2005, **50**, 1727–1732.
28 S. Hartwig and H. Hillebrecht, Crystal Structures of $NbOI_3$ and $NbOBr_3$ – Polar Double Chains in Different Non-Centrosymmetric Structures, *Z. Anorg. Allg. Chem.*, 2008, **634**(1), 115–120.
29 B. S. Ault, Infrared Matrix Isolation Study of the 1:1 Molecular Complex of $OVCl_3$ with $(CH_3)_2O$, *Spectrochim. Acta, Part A*, 2003, **59**, 1989–1994.
30 M. D. Hoops and B. S. Ault, Matrix Isolation Infrared Spectroscopic Investigation of the Coordination Chemistry and Reactivity of OVF_3, *J. Mol. Struct.*, 2002, **616**, 91–101.
31 M. J. Frisch, G. W. Trucks, H. B. Schlegel, G. E. Scuseria, M. A. Robb, J. R. Cheeseman, G. Scalmani, V. Barone, G. A. Petersson and H. Nakatsuji, *Gaussian 16, rev. C.02*, Gaussian, Inc., Wallingford, CT, 2019.
32 J.-D. Chai and M. Head-Gordon, Long-range corrected hybrid density functionals with damped atom-atom dispersion corrections, *Phys. Chem. Chem. Phys.*, 2008, **10**, 6615–6620.
33 R. A. Kendall, T. H. Dunning Jr. and R. J. Harrison, Electron Affinities of the First-row Atoms Revisited. Systematic Basis Sets and Wave Functions, *J. Chem. Phys.*, 1992, **96**, 6796–6806.

34 D. E. Woon and T. H. Dunning Jr, Gaussian Basis Sets for Use in Correlated Molecular Calculations. III. The Atoms Aluminum through Argon, *J. Chem. Phys.*, 1993, **98**, 1358–1371.
35 M. Dolg, U. Wedig, H. Stoll and H. Preuss, Energy-adjusted *Ab Initio* Pseudopotentials for the First Row Transition Elements, *J. Chem. Phys.*, 1987, **86**, 866–872.
36 K. A. Peterson, D. Figgen, E. Goll, H. Stoll and M. Dolg, Systematically Convergent Basis Sets with Relativistic Pseudopotentials. II. Small-Core Pseudopotentials and Correlation Consistent Basis Sets for the Post-d Group 16–18 Elements, *J. Chem. Phys.*, 2003, **119**, 11113–11123.
37 K. A. Peterson, B. C. Shepler, D. Figgen and H. Stoll, On the Spectroscopic and Thermochemical Properties of ClO, BrO, IO, and Their Anions, *J. Phys. Chem. A*, 2006, **110**, 13877–13883.
38 K. A. Peterson, D. Figgen, M. Dolg and H. Stoll, Energy-Consistent Relativistic Pseudopotentials and Correlation Consistent Basis Sets for the 4d Elements Y–Pd, *J. Chem. Phys.*, 2007, **126**, 124101.
39 D. Figgen, K. A. Peterson, M. Dolg and H. Stoll, Energy-Consistent Pseudopotentials and Correlation Consistent Basis Sets for the 5d Elements Hf–Pt, *J. Chem. Phys.*, 2009, **130**, 164108.
40 Energy-consistent pseudopotentials of the Stuttgart-Cologne group. **https://www.tc.uni-koeln.de/PP/clickpse.en.html** (last accessed August 28, 2025).
41 J. M. Martin and A. Sundermann, Correlation Consistent Valence Basis Sets for Use with the Stuttgart–Dresden–Bonn Relativistic Effective Core Potentials: The Atoms Ga–Kr and In–Xe, *J. Chem. Phys.*, 2001, **114**(8), 3408–3420.
42 R. Dennington, T. A. Keith and J. M. Millam, *GaussView, 6.0*, Semichem Inc., Shawnee Mission, KS, 2016.
43 T. Lu and F. Chen, Multiwfn: a multifunctional wavefunction analyzer, *J. Comput. Chem.*, 2012, **33**, 580–592.
44 T. Lu and F. Chen, Quantitative analysis of molecular surface based on improved Marching Tetrahedra algorithm, *J. Mol. Graphics Modell.*, 2012, **38**, 314–323.
45 Chemcraft – Graphical Software for Visualization of Quantum Chemistry Computations **https://www.chemcraftprog.com**.
46 B. S. Ault, Matrix isolation study of the thermal and photochemical reaction of $OVCl_3$ with NH_3: Spectroscopic and theoretical characterization of $Cl_2V(O)NH_2$, *J. Phys. Chem. A*, 2001, **105**, 4758–4764.
47 P. Pyykkö and M. Atsumi, Molecular Single-Bond Covalent Radii for Elements 1–118, *Chem. – Eur. J.*, 2009, **15**, 186–197.
48 S. S. Batsanov, *Inorg. Mater.*, 2001, **37**, 871–885 (translated from *Neorg. Mater.*, 2001, **37**, 1031–1046). We use here for consistency the crystallographic van der Waals radii for all of the elements in question as presented in Table 9 of this reference.
49 NIST Inorganic Crystal Structure Database, NIST Standard Reference Database Number 3, National Institute of Standards and Technology, Gaithersburg MD, 20899, DOI: **10.18434/M32147**, (retrieved August 2025).
50 Crystal structure images were generated using CrystalMaker®: a crystal and molecular structures program for Mac and Windows. CrystalMaker Software Ltd, Oxford, England (**https://www.crystalmaker.com**).
51 I. Nowak, E. M. Page, D. A. Rice, A. D. Richardson, R. J. French, K. Hedberg and J. S. Ogden, Chalcogenide-Halides of Niobium(v). 1. Gas-Phase Structures of $NbOBr_3$, $NbSBr_3$, and $NbSCl_3$. 2. Matrix Infrared Spectra and Vibrational Force Fields of $NbOBr_3$, $NbSBr_3$, $NbSCl_3$, and $NbOCl_3$, *Inorg. Chem.*, 2003, **42**, 1296–1305.
52 A version of the C_{2v} doubly bridged dimer (see Fig. 3(iii)) is obtained for $(MOH_3)_2$, but it is very distorted for M = Ta (see also the.xyz coordinates for the MOH_3 dimer in the SI).
53 The computed Nb═O double bond distance in the $NbOCl_3$ molecule is 1.668 Å (comparable to 1.693(4) from experiment), and the Nb–O single bond in the computed trigonal bipyramidal $NbCl_4OH$ molecule is 1.863 Å, which is still much shorter than the computed inter-dimer distance of 2.573 in the tetramer or even the experimental 2.203 Å in the extended solid.

